Journal of Nanostructure in Chemistry (2021) 11:751–767
https://doi.org/10.1007/s40097-021-00401-0

ORIGINAL RESEARCH

Design and synthesis of a new magnetic aromatic organo-silane star polymer with unique nanoplate morphology and hyperthermia application

Reza Eivazzadeh-Keihan[1] · **Ali Maleki**[1]

Received: 9 November 2020 / Accepted: 5 April 2021 / Published online: 12 April 2021

Abstract

In this study, new statistical magnetic organo-silane star polymers were designed, synthesized based on different surface functionalization processes of Fe_3O_4 magnetic nanoparticles and conducting the polymerization reaction between phenylenediamine derivatives and dichlorophenylsilane on their functionalized surfaces. Fourier-transform infrared (FT-IR) spectroscopy, energy-dispersive X-ray (EDX), field-emission scanning electron microscope (FE-SEM) and transmittance electron microscope (TEM) images, X-ray diffraction (XRD) pattern, thermogravimetric (TG) analysis, vibrating-sample magnetometer (VSM), and dynamic light-scattering (DLS) and zeta potential measurements were employed to characterize the structural features. Based on the MTT assay and considering the highest concentration (1000 μg mL^{-1}) of statistical magnetic organo-silane star polymer based on *p*-phenylenediamine as model derivative, the cell viability percentage of was reported 89.7%. In addition, the hyperthermia performance of this magnetic star polymer was evaluated by its exposure to an alternating magnetic field (AMF). Given the obtained results from different concentrations, the highest specific absorption rate (66.18 W g^{-1}) was determined for 0.5 mg mL^{-1} of prepared sample. Therefore, it can be concluded that this new magnetic nanocomposite can be considered as an efficient agent for the next generation of therapeutic researches.

✉ Ali Maleki
maleki@iust.ac.ir

[1] Catalysts and Organic Synthesis Research Laboratory, Department of Chemistry, Iran University of Science and Technology, Tehran 16846-13114, Iran

Graphic abstract

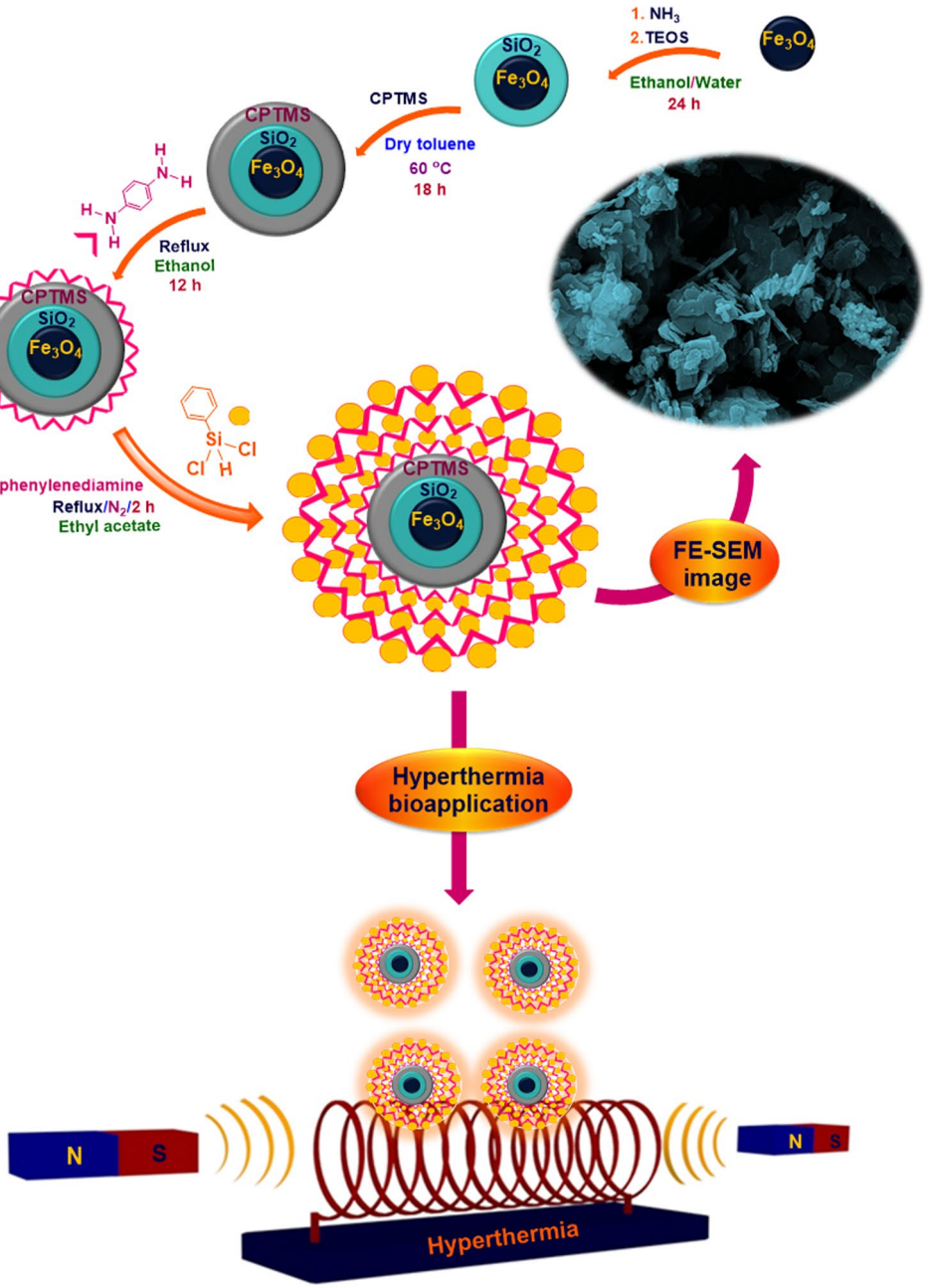

Keywords Organo-silane polymer · Magnetic nanoparticles · Nanoplate morphology · Hyperthermia · Specific absorption rate

Introduction

In the last decade, due to emergence of advanced and controlled polymerization techniques, wide range of polymeric macromolecules have been synthesized with controlled dimension, specific functionality and unique features [1]. Among different polymeric macromolecules, star-shaped polymers with owning an exclusive structure including a central core and linear polymeric branches (arm) which are fused to the central point (core) have been created a unique class of multifunctional nanomaterials, which are currently applied in various and extensive fields such as

nanotechnology, medical, material sciences, and industrial settings [1, 2]. The classification of these macromolecular architectures can be conducted due to monomer composition, chemistry or nature of the central core, sequence distribution of arm polymer and functional placement [1]. In addition, various strategies have been applied in the synthesis process of star-shaped polymers, which can be classified into three different strategies including core-first, arm-first, and grafting onto strategies [1, 3]. In this regard, Fe_3O_4 magnetic nanoparticles (Fe_3O_4 MNPs) are one of the most qualified nanoparticles which have enticed a great deal of interests due to their specific and unique physiochemical features such as high surface-to-volume ratio, superparamagnetism, high magnetic susceptibility, low curie temperature, high coercivity, and being easily separated from reaction system [4, 5]. These forefront nanoparticles with having exclusive size-dependent properties have been converted to one of the most indispensable and superior materials in various fields including catalysis [6–9], nanotechnology and biomedicine [5, 10, 11]. On the other hands, their imperative role as core of synthesized nanomaterials, the ease of their surface functionalization processes, grafting of synthetic and natural molecules and generation of unique magnetic nanostructural composites have been extended their application. For instance, in order to identify pathogenic viruses [12, 13], toxic proteins [14, 15], different mycotoxins [16], and antifungal medications cancer biomarkers [17]. As well as, a diversity of paramagnetic scaffolds with owning efficient biological performance have been approved and utilized in tissue engineering [18]. Following these descriptions, one of the most notable therapeutic methods which has been employed in cancer treatment, is adjunctive hyperthermia therapy. In recent years, the combination of hyperthermia with conventional methods including surgery, radiotherapy, chemotherapy and immunotherapy has improved the therapeutic process of advanced and recurrent cancers [19]. In this field, current hyperthermia strategies are classified into local, regional and whole-body hyperthermia. These three strategies can be performed by various heating methods such as microwave, laser, radiofrequency, and ultrasound techniques [19].

Recently, applying magnetic nanoparticles and their functionalization with various coating shells or targeting agents have been considered as a new therapeutic heating method [20, 21]. In the hyperthermia process, due to employing an alternating magnetic field (AMF) and considerable increment in intracellular local temperature by magnetic nanomaterials movements, the cancerous cells are destroyed [20–23]. Surface functionalization of Fe_3O_4 MNPs is required to promote their biocompatibility, colloidal stability in different biocompatible mediums, and avoiding their aggregation due to the interparticle magnetic forces [24]. Also, Fe_3O_4 MNPs alone show high chemical activity on their surfaces but on the other side, they are susceptible to oxidize in the air. Oxidization of these magnetic nanoparticles can reduce their magnetization and dispersibility [25]. Therefore, their surface functionalization must be considered as an imperative solution to enhance their biological performance and colloidal stability [25]. In this respect, given the recent studies, it has determined that surface functionalization of Fe_3O_4 MNPs by natural and synthetic polymers can improve their colloidal stability in water due to the creation of steric stabilization [26]. So far, the surface of Fe_3O_4 MNPs has functionalized by diversity of natural and synthetic polymers such as chitosan [25, 27, 28], cellulose [29], agar [30], pectin [31], alginate [32], gelatin [33], polyvinylidene fluoride [34], polypyrrole [35], and casein [36]. The grafting process on the surface of Fe_3O_4 MNPs can be carried out by wide range of anchor molecules such as dopamine, cysteine, carboxylic acid, trimethoxysilane, and phosphonic acid. The existence of these molecules on the surface of Fe_3O_4 MNPs can provide better condition for chemical interactions and the generation of new covalent and non-covalent bonds [26]. Alongside surface functionalization and synthesis of new core–shell nanostructures, the polymerization reaction and growth of polymer can also be conducted on the surface of Fe_3O_4 MNPs to synthesis magnetic star-shaped polymers. In these kind of reaction conditions, magnetic nanoparticles act as core of star-shaped polymers and magnetic star-shaped polymeric structures are synthesized [37–39]. As an example, taking into account the copper-mediated atom transfer radical polymerization method, the graft polymerization of methyl methacrylate on the surface of Fe_3O_4 MNPs is accomplished using an initiator. The polymerization process is such a way that the Fe_3O_4 MNPs show exceptional stability and as well, their dispersibility was improved in organic solvent [37, 40, 41]. In another example, biocompatible and amino-functionalized superparamagnetic iron-oxide nanoclusters have synthesized using ring-opening polymerization technique. These magnetic nanoclusters demonstrate low cytotoxicity and considerable stability in aqueous solutions. As well as, these magnetic nanoclusters have considered as a favorable magnetic resonance imaging (MRI) contrast agents due to their effective folate-receptor (FR)-mediated uptake [38].

According to the importance of magnetic star-shaped nanostructures and in the best of our knowledge, unique statistical magnetic organo-silane star polymers are introduced. In this study, considering the functionalized surface of Fe_3O_4 MNPs, the polymerization reaction is accomplished between the phenylenediamine derivatives and dichlorophenylsilane (Scheme 1). Among these synthesized magnetic nanocomposites, the magnetic nanostructure based on *p*-phenylenediamine as a model nanocomposite is characterized. In addition, its performance is evaluated by applying alternating magnetic field (AMF).

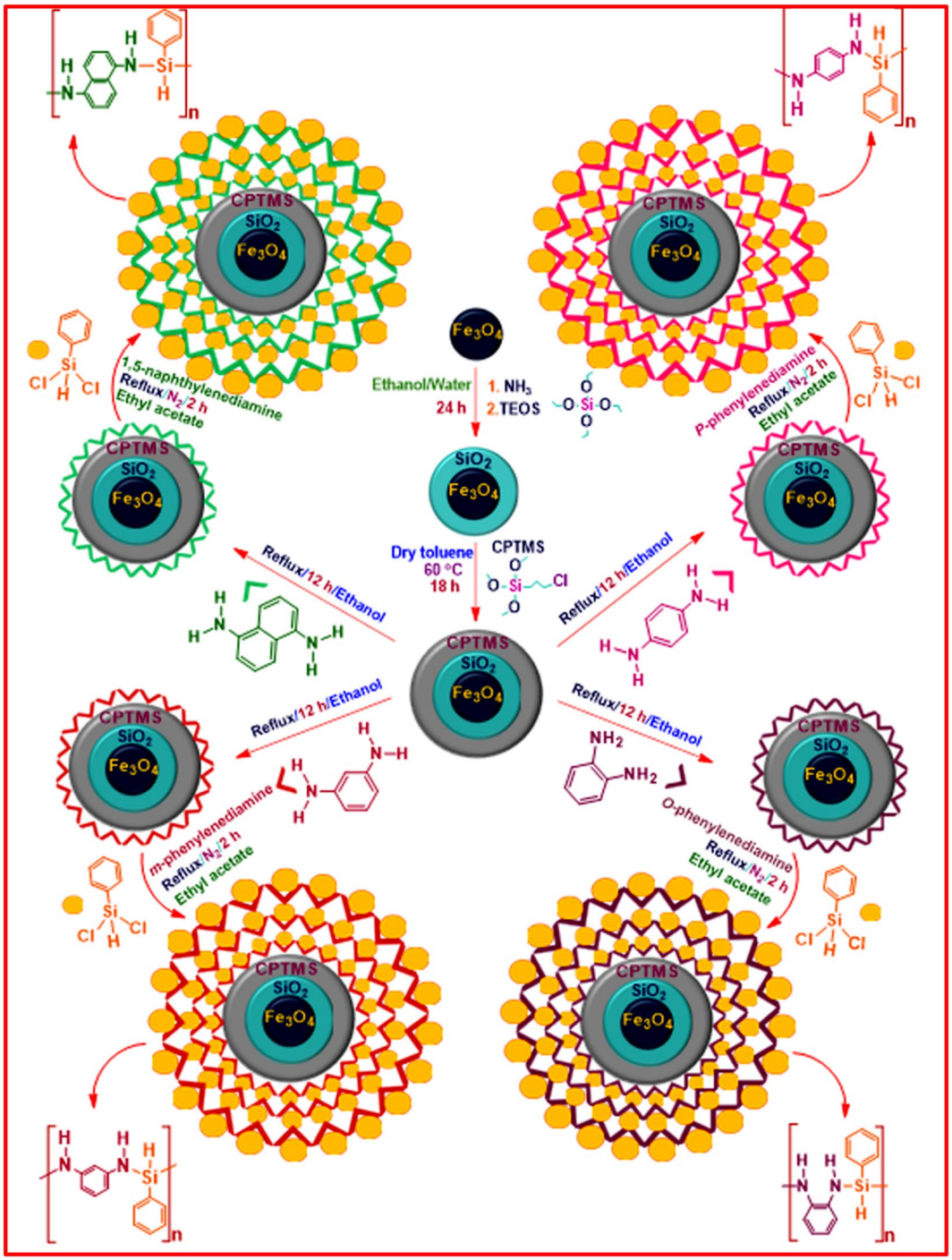

Scheme 1 Schematic process of polymerization reaction between phenylenediamine derivatives and dichlorophenylsilane on the surface of functionalized Fe_3O_4 MNPs

Experimental section

General

All the solvents and reagents as required chemical materials, with high purities were purchased from the international chemical companies such as Merck, Fluka and Sigma-Aldrich. To characterize the statistical magnetic organosilane star polymers and concede the synthesis and growth of polymer on the surface of Fe_3O_4 MNPs, Fourier-transform infrared (FT-IR) spectra were taken using KBr pellets method (Shimadzu IR-470 model, Japan). Energy-dispersive

X-ray (EDX) analysis was carried out using Numerix DXP-X10P (France). The morphology, size and structure of designed magnetic nanocomposites were recorded by field-emission scanning electron microscope (FE-SEM) (ZEISS-sigma VP model, Germany) and transmittance electron microscope (TEM) (ZEISS-EM10C-100KV, Germany). The X-ray diffraction (XRD) pattern was characterized by Bruker device (D8 advance model, Germany). The vibrating-sample magnetometer (VSM) was taken by LBKFB model-magnetic Kashan kavir (Iran) (5000 Oe). As well as, to evaluate its thermogravimetric behavior thermal consistency, the TG analysis was taken by Bahr-STA 504 (Germany). This analysis was performed under the argon atmosphere with 5.0 mg of nanocomposite in alumina pans. 3-(4,5-Dimethyl-2-thiazolyl)-2,5-diphenyl-2H-tetrazolium bromide (MTT) assay was conducted by using microplate reader (STAT FAX 2100, BioTek, Winooski, USA) and the absorbance was measured at 545 nm. to evaluate the heating power of the magnetic aromatic organo-silane star polymer, during the 5- to 20-min intervals, different concentrations of designed magnetic nanocomposite (0.5 mg mL^{-1}, 1 mg mL^{-1}, 2 mg mL^{-1}, 5 mg mL^{-1}, 10 mg mL^{-1}) were exposed to AMF with different frequencies (100 MHz, 200 MHz, 300 MHz, 400 MHz).

Preparation of Fe_3O_4 MNPs

As mentioned in previous literatures about the preparation of Fe_3O_4 MNPs using coprecipitation methods [2, 42], in the first step, 2.91 of $FeCl_3{\cdot}6H_2O$ and 1.33 g of $FeCl_2{\cdot}4H_2O$ salts were dissolved in 80 mL of distilled water. Afterward, the obtained mixture solution was stirred under N_2 atmosphere. Then, the mixture solution was heated up to 70 °C. Following the constant temperature condition (70 °C), 10 mL of aqueous ammonia solution (25%) was added drop wisely to the mixture solution. In the next step, the mixture solution was stirred in the constant temperature (70 °C) for 2 h. After the mentioned time and cooling the mixture solution, using an external magnet, the obtained black precipitate was separated and washed with distilled water for several times (supplementary information Fig. S1).

Surface functionalization of Fe_3O_4 MNPs using silica shell (Fe_3O_4@SiO_2)

Based on Stöber method with some modification and reformations [43] and previous studies about functionalization of Fe_3O_4 MNPs [2, 42], the surface functionalization process of Fe_3O_4 MNPs using silica shell was achieved by these steps. Primarily, using the ultrasonic bath, 0.22 g of synthetic Fe_3O_4 MNPs was dispersed into 50 mL of distilled water for 20 min. After the mentioned time, under the stirring condition, 7.5 mL of ammonia solution (25%) was drop wisely added. Next, after adding 80 mL of ethanol, subsequently, a determined amount of tetraethyl orthosilicate (TEOS) solution (4 mL) was gently added to the mentioned suspension solution. After 24 h, the functionalized Fe_3O_4 MNPs were separated and washed with distilled water and ethanol. As well as, to have dried product, it was kept in an oven (70 °C) for an overnight (supplementary information Fig. S2).

Second surface functionalization of Fe_3O_4@SiO_2 MNPs by CPTMS shell (Fe_3O_4@SiO_2-Cl)

To functionalize the surface of Fe_3O_4@SiO_2 MNPs by (3-chloropropyl)trimethoxysilane (CPTMS) molecules as second shell [2], first, under the mechanical stirring condition, 0.69 g of functionalized Fe_3O_4 MNPs was dispersed in 100 mL of dried toluene at 60 °C. After mixing the functionalized Fe_3O_4 MNPs with dried toluene, 1 mL of CPTMS solution was drop wisely added to the mixture solution. The suspension solution was stirred mechanically for 18 h at 60 °C. Finally, the separation of obtained magnetic product was done using an external magnet and dried in a vacuum oven (supplementary information Fig. S3).

Third surface functionalization of Fe_3O_4@SiO_2-Cl MNPs by phenylenedamine derivatives shell (Fe_3O_4@SiO_2-phenylenediamine)

The third surface functionalization of Fe_3O_4@SiO_2-Cl MNPs was accomplished by phenylenediamine derivative molecules [2]. In this respect, initially, 2 mmol of phenylenediamine derivative was dissolved in 25 mL of ethanol. After dissolution, 1.00 g of Fe_3O_4@SiO_2-Cl MNPs was added to the mixture solution and then, the suspension solution was refluxed (80 °C) for 12 h. After the mentioned time, the phenylenediamine-functionalized Fe_3O_4 MNPs was separated and it was washed with ethanol. Finally, the obtained solid product was kept in the oven at 80 °C for 12 h (supplementary information Fig. S4).

Polymerization on the surface of functionalized Fe_3O_4 MNPs (Fe_3O_4@SiO_2-polymer)

Conducting the polymerization reaction on the surface of functionalized Fe_3O_4 MNPs and synthesis of statistical magnetic organo-silane star polymer was carried out by these steps. In the first step, under the ultrasonic irradiation, 1.00 g of obtained magnetic functionalized core was dispersed in 50 mL of ethyl acetate. Afterward, 10 mmol of phenylenediamine derivative was appended to the solution. After the 20 min, 10 mmol of dichlorophenylsilane solution was slowly added to the suspension solution during 1 h. After adding dichlorophenylsilane reagent, the suspension solution was kept under the mechanical stirring condition at

room temperature for 5 h. In the next step, the suspension solution was kept under the reflux condition (80 °C) and N_2 atmosphere for 2 h. After the mentioned time, the polymer-functionalized Fe_3O_4 MNPS was separated from reaction solution and then, it was washed with ethyl acetate. Finally, the synthetic magnetic nanocomposite was placed in the oven at 70 °C for 12 h (supplementary information Fig. S5).

Results and discussion

In this study, functionalization of Fe_3O_4 MNPs surface by various inorganic and organic shells and conducting the polymerization reaction between phenylenediamine derivatives and dichlorophenylsilane on their surfaces, new magnetic nanocomposites have been generated with considerable and specific features. As determined in Scheme 1, the fabrication of these statistical magnetic organo-silane star polymers is accompanied by five synthesis steps. The first step is fabrication of synthetic Fe_3O_4 MNPs. The third synthetic steps are included their surface functionalization using inorganic TEOS, CPTMS and organic phenylenediamine derivatives shells and as well as, the final synthetic step is the polymerization reaction between phenylenediamine derivatives and dichlorophenylsilane on the functionalized surface of Fe_3O_4 MNPs. Considering the structure of polymeric shells (dichlorophenylsilane and phenylenediamine derivative monomers), it can be deduced that these designed magnetic nanocomposites are classified as statistical magnetic organo-silane star polymers. Alongside of their synthesis process, a diversity of spectral and analytical techniques was employed to concede and characterize the structure of these magnetic nanostructures and as well their features. FT-IR spectrum of each synthesis step and determination of new functional groups, detection of structural elements by EDX analysis, applying FE-SEM and TEM images to characterize the morphology, size and structure of designed magnetic nanocomposite, XRD pattern, TG, VSM analyses to evaluate its thermal stability and magnetic property, and as well DLS and zeta potential measurements are, respectively, discussed in this part.

Characterization of designed statistical magnetic organo-silane star polymer

FT-IR analysis

The fabrication process of designed statistical magnetic organo-silane star polymer based on *p*-phenylenediamine was confirmed by applying FT-IR spectral technique in each synthesis step and new absorption bands (Fig. 1a–e). As could be seen, the FT-IR spectrum of Fe_3O_4 MNPs is indicated in Fig. 1a. An absorption band around 569 cm^{-1} is attributed to the Fe–O stretching vibration mode of magnetic nanoparticles [44]. The presence of a broad band at 3400 cm^{-1} confirms the stretching vibration of hydroxyl groups on the surface of Fe_3O_4 MNPs [45]. The first surface functionalization process of Fe_3O_4 MNPs by alkoxysilane molecules of TEOS is characterized by generation of new functional groups (Fig. 1b). As illustrated in Fig. 1b, first of all, the O–H stretching vibration mode is assigned by observing a broad band at the range of 3200–3600 cm^{-1} [46]. The bending vibration mode of Si–O–Si and two Si–O–Si asymmetric and symmetric vibration modes are, respectively, related to three new absorption bands around 479 cm^{-1}, 1100 cm^{-1} and 800 cm^{-1}. As well as, the O–H stretching vibration mode of Si–OH and twisting vibration mode of adsorbed H–O–H in silica shell are determined by a peak around 1637 cm^{-1} [45–47]. Figure 1c is related to the grafting reaction of CPTMS molecules as second layer on the functionalized surface of Fe_3O_4 MNPs (Fe_3O_4@SiO_2). As indicated in Fig. 1c, the interaction between CPTMS molecules and existent SiO_2 layer on the surface of Fe_3O_4 MNPs are confirmed by observing two weak absorption bands around 1410 cm^{-1} and 2855 cm^{-1}; which are characterized as Si–CH_2 and CH_2 stretching vibration modes [48]. The third surface functionalization process between *p*-phenylenediamine molecules and functionalized magnetic nanoparticles is determined by observing new absorption bands (Fig. 1d). As illustrated in Fig. 1d, observing a broad absorption band around 3200–3600 cm^{-1} is ascribed to the N–H stretching vibration mode of second amine which has overlap with the N–H stretching vibration mode of first amine. the C=C stretching vibration mode of quinonoid and benzenoid rings and the C–N stretching vibration mode of benzenoid ring are assigned by two absorption bands around 1600 cm^{-1} and 1490 cm^{-1}, and a small band around 1317 cm^{-1}. As well as, Si–O–Si absorption band has covered the absorption band of N=Q=N (quinonoid ring is represented by Q) [49]. Conducting the polymerization reaction on the surface of functionalized Fe_3O_4 MNPs is recognized by confirming new functional groups (Fig. 1e). An absorption band around 1430 cm^{-1} is attributed to phenyl-Si stretching vibration mode [50]. The fabricated Si–N band and its stretching vibration mode is characterized by observing an absorption band around 1550 cm^{-1} [51]. A weak absorption band around 2170 cm^{-1} can be ascribed to Si–H vibration mode [52]. Observing a sharp absorption band around 1504 cm^{-1} confirms the N–H bending vibration mode. Following that, an absorption band 1627 cm^{-1} is ascribed to C=C stretching vibration mode of attached phenyl group of silicon, which has covered the C=C stretching vibration bands of benzenoid and quinonoid rings [52]. In addition, it should be mentioned that the FT-IR spectra (final synthesis step)

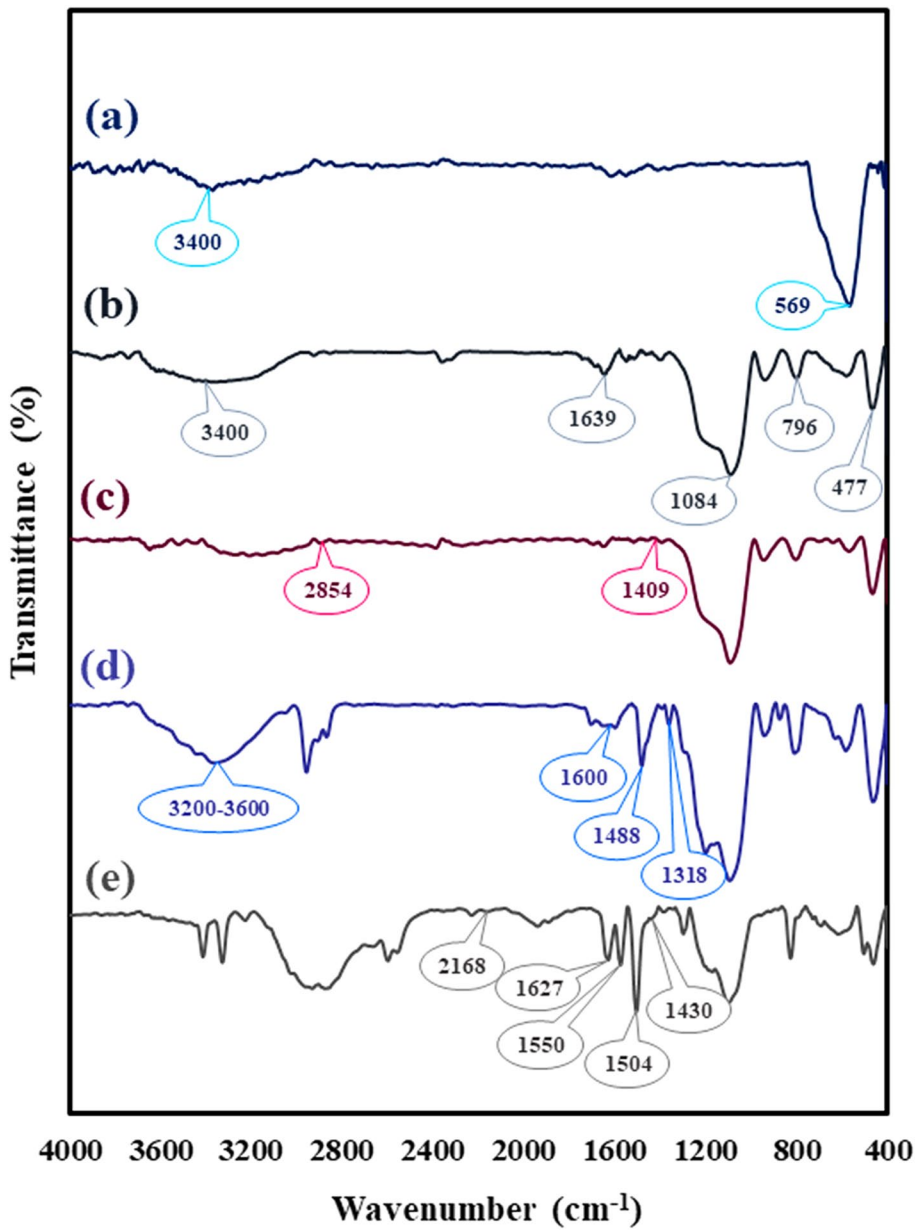

Fig. 1 FT-IR spectra of **a** unfunctionalized Fe_3O_4 MNPs, **b** Fe_3O_4@SiO_2, **c** Fe_3O_4@SiO_2@CPTMS, **d** Fe_3O_4@SiO_2@CPTMS@PPD (*p*-phenylenediamine) and **e** statistical magnetic aromatic organo-silane star polymer based on *p*-phenylenediamine (core–shell)

of other derivative nanocomposites can be observed in the supplementary information file (supplementary information Figs. S6, S7, S8).

EDX analysis

Taking into account the qualitative EDX analysis for determination of structural elements of diverse organic and inorganic compounds, the EDX spectrum of designed statistical magnetic aromatic organo-silane star polymer based on *p*-phenylenediamine is indicated in Fig. 2. As illustrated, based on functionalization processes on surface of Fe_3O_4 MNPs, synthesis and growth of designed polymer and as well the observed results from elemental detection, it is deduced that the presence of two iron peaks can be attributed to the synthetic Fe_3O_4 MNPs. Intense silicon peak can be implied to the coated TEOS, CPTMS shells and as well dichlorophenylsilane which is one of the main reactants of synthesized polymer. Alongside of iron and silicon peaks, two carbon and nitrogen can be related to the growth and synthesis of polymer due to structure of two *p*-phenylenediamine and dichlorophenylsilane reagents. Also, it should be mentioned that the EDX spectrum other derivative nanocomposites can be observed in the supplementary information file (supplementary information Figs. S9, S10, S11).

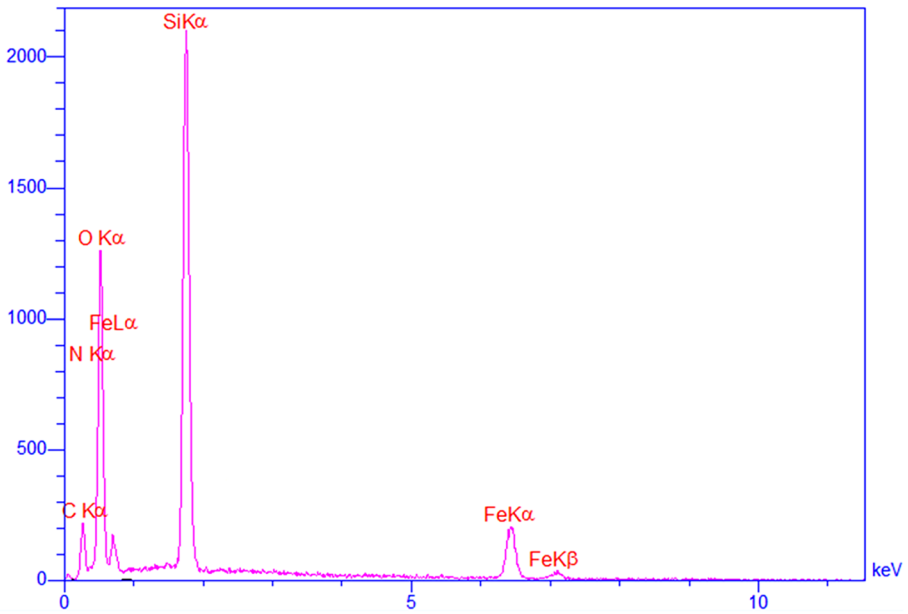

Fig. 2 EDX spectrum of statistical magnetic aromatic organo-silane star polymer based on *p*-phenylenediamine due to polymerization reaction between *p*-phenylenediamine and dichlorophenylsilane

FE-SEM imaging

As could be seen, the FE-SEM images of statistical magnetic aromatic organo-silane star polymer based on *p*-phenylenediamine are shown in Fig. 3a and b. Due to functionalization processes on the surface of Fe_3O_4 MNPs and specially conducting the polymerization reaction between *p*-phenylenediamine and dichlorophenylsilane, in a precise investigation, it has determined that nanoplate structures have generated layer by layer. As well as, the arrangement of these nanoplate structures is such a way that the surface of Fe_3O_4 MNPs has well covered (core–shell structure). In

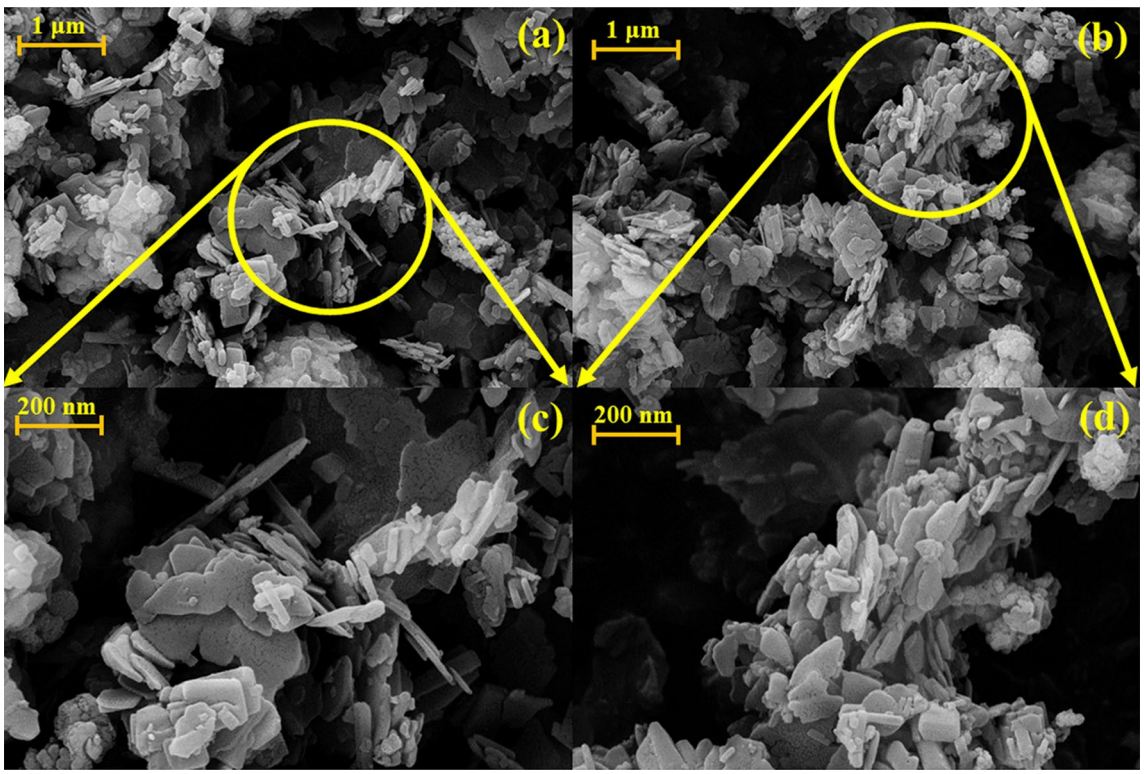

Fig. 3 **a–d** FE-SEM images of statistical magnetic aromatic organo-silane star polymer based on *p*-phenylenediamine

addition, it should be mentioned that the FE-SEM images of other derivative nanocomposites can be observed in the supplementary information file (supplementary information Figs. S12, S13, S14, S15).

TEM imaging

According to the obtained results from TEM imaging (Fig. 4) and considering the structure of magnetic aromatic organo-silane star polymer based on *p*-phenylenediamine, the sphere morphology for Fe_3O_4 cores is well characterized. Besides, due to the polymerization reaction, the TEM image has confirmed that these sphere magnetic cores are covered by a vast shell which is attributed to the polymeric matrix shell.

XRD pattern

The XRD pattern of designed statistical magnetic aromatic organo-silane star polymer based on *p*-phenylenediamine is indicated in Fig. 5a and b. Considering the observed diffraction angles ($2\theta = 14.51$, 19.85, 21.15, 24.01, 26.34, 29.27, 30.19, 33.28, 34.16, 40.31, 42.30, 43.21, 44.47, 48.40, 49.77, 55.36, 62.85), all the crystalline bands are matched with XRD pattern of Fe_3O_4 MNPs (JCPDS card No. 01-076-0958).

Thermogravimetric analysis

The thermogravimetric behavior and thermal stability of designed statistical magnetic aromatic organo-silane star polymer were evaluated by applying TG analysis. The decomposition of magnetic aromatic organo-silane star polymer is indicated in obtained thermogravimetric curve (Fig. 6). As could be seen in Fig. 6, in a close and precise investigation, the first mass reduction (50–250 °C) which is almost 7%, is related to the existence of absorbed solvent molecules and as well the presented impurities in the structure of designed magnetic nanocomposite [2]. Following the first mass reduction, a second mass reduction (almost 28%) is observed at temperature range of 250 °C to almost 370 °C which is considered for cleavage of grafted linkers and organic moieties [53]. The notable third mass reduction (30%) at temperature range of 370 °C to almost 700 °C can be attributed to the partial decomposition of synthesized polymer. As this organo-silane polymer is new, the fourth mass reduction (almost 7%) at temperature range of 700–850 °C can be related to the destruction of other organic compounds, which are obtained from the decomposition of synthesized polymer. Besides, it should be mentioned that the thermogravimetric curves of other derivative nanocomposites can be observed in the supplementary information file (supplementary information Figs. S16, S17, S18).

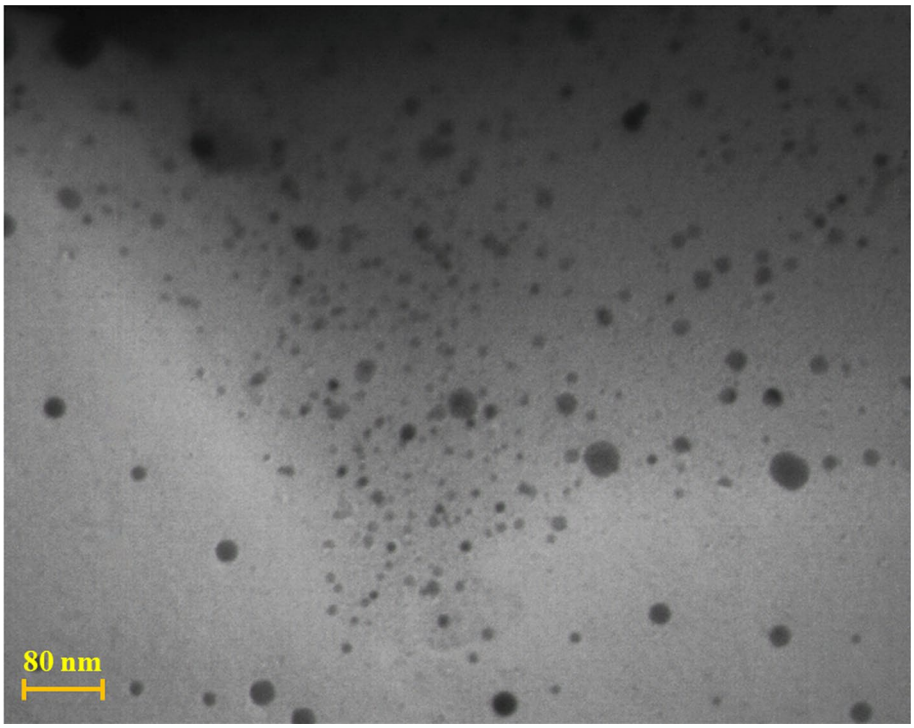

Fig. 4 TEM image statistical magnetic aromatic organo-silane star polymer based on *p*-phenylenediamine

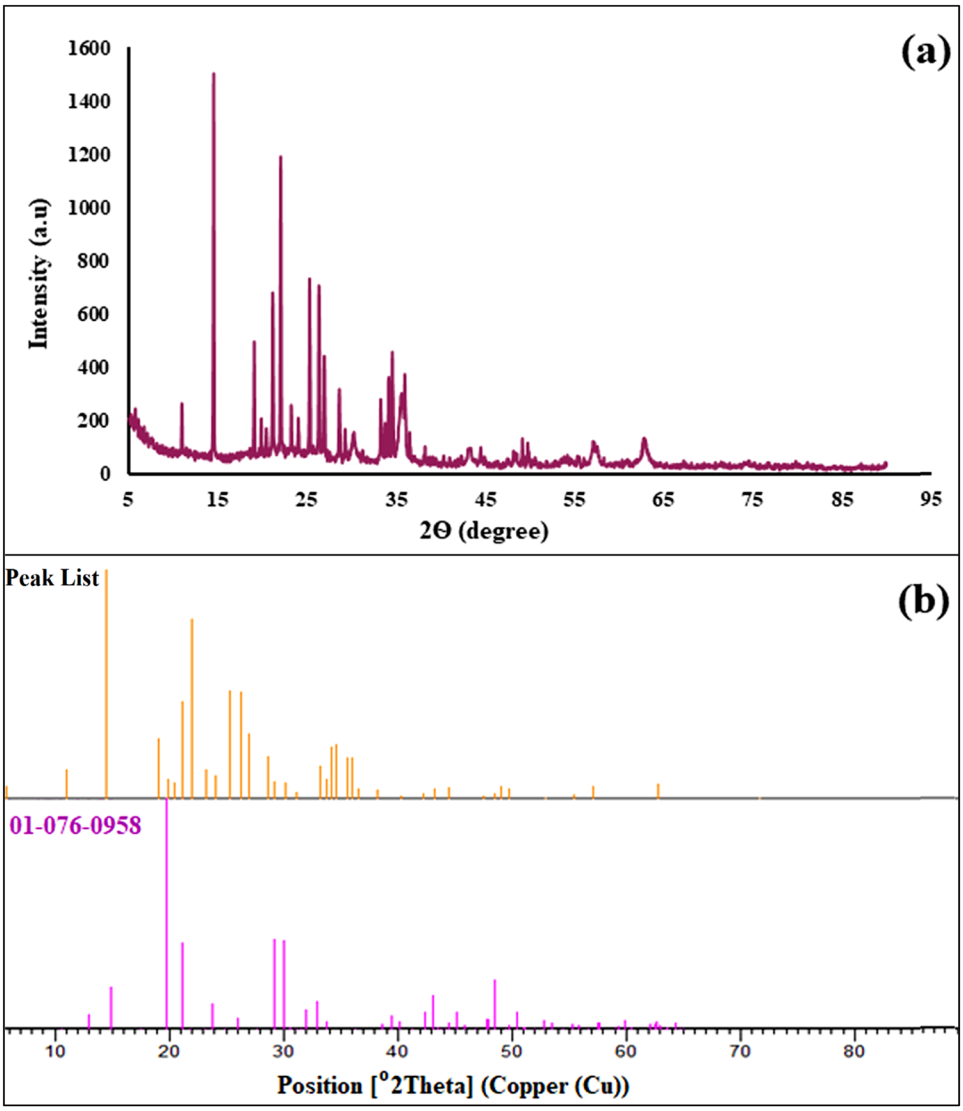

Fig. 5 **a** XRD pattern of magnetic aromatic organo-silane star polymer based on *p*-phenylenediamine and **b** reference of synthetic Fe_3O_4 MNPs in the structure of designed magnetic nanocomposite

VSM analysis

Principally, distinctive parameters including core size, interparticle distance, shell thickness, iron-group crystalline structure and interparticle and intraparticle interactions can take part an imperative role in magnetic characteristics of magnetic materials [54]. As well as, according to the previous reported studies, it was approved that the synthesis of Fe_3O_4-based nanocomposites and their surface functionalization processes can reduce the value of saturation magnetization [2]. The hysteresis loop curves of unmodified and designed magnetic statistical magnetic aromatic organo-silane star polymer are illustrated in Fig. 7a and b. According to the obtained saturation magnetization values (Ms) by applying vibrating-sample magnetometer, the saturation magnetization values of unmodified Fe_3O_4 MNPs (76.20 emu g^{-1}) and designed magnetic nanocomposite (10.41 emu g^{-1}) were determined. On the other hand, comparing the results indicated that the value of saturation magnetization has reduced dramatically (Fig. 7b). Based on this significant reduction, it can be concluded that functionalization processes, synthesis and growth of organo-silane polymer have well accomplished.

DLS and zeta potential measurements

According to the DLS results, it has indicated that the average size of nanoparticles with the distribution ranging from 29.39 to 95.07 nm, is 43 nm in water (Fig. 8a). As well as, the *Z*-average is 509.4 (r,nm) with PDI around 0.439. The nanoparticle's zeta potential (surface charge) data determine how stable or aggregated colloids can be formed by nanoparticles during the colloidal phase. At low zeta potential, the repulsion of nanoparticles is not occurred strongly and given the attractive surface forces, the colloids will be aggregated. In contrast, considering the high zeta potential

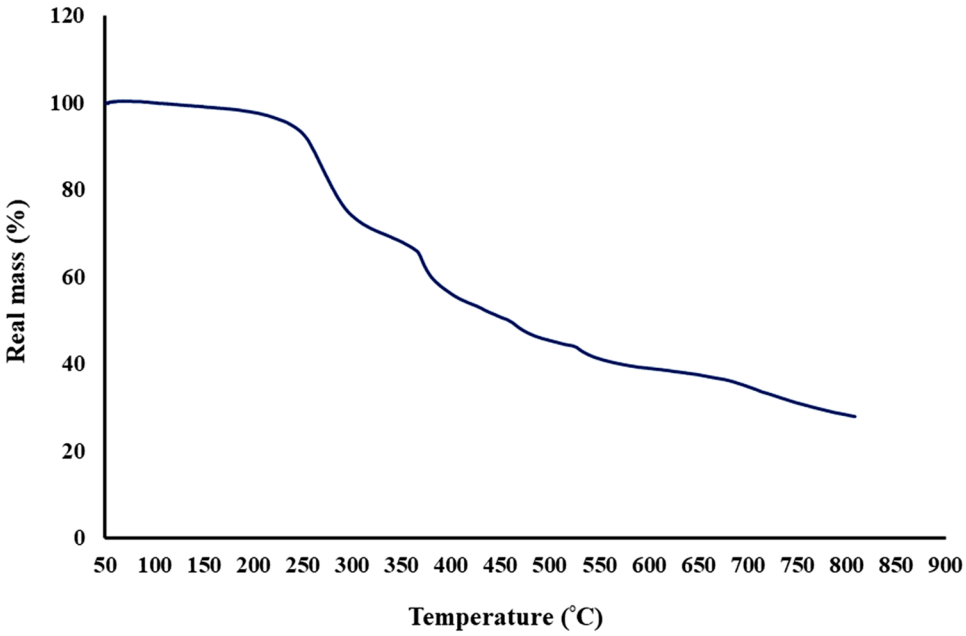

Fig. 6 Thermogravimetric curve of statistical magnetic aromatic organo-silane star polymer due to polymerization reaction between *p*-phenylenediamine and dichlorophenylsilane on the surface of functionalized Fe_3O_4 MNPs

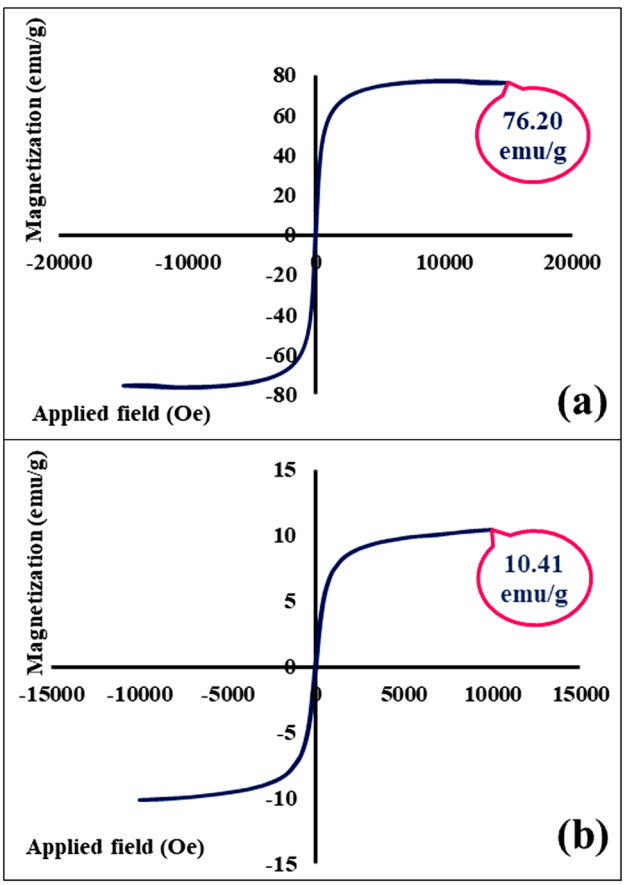

Fig. 7 Hysteresis loop curve of **a** unmodified Fe_3O_4 MNPs and **b** magnetic aromatic organo-silane star polymer based on *p*-phenylenediamine

(above ~ 30 mV), the stable dispersions of nanoparticles are formed. High zeta potential as an important factor in water treatment and biomedical applications, is required for stable colloidal systems [55]. According to the zetapotential results, it has indicated that the zeta potential of magnetic aromatic organo-silane star polymer based on *p*-phenylenediamine is 35.2 mV; which it can be concluded that this magnetic nanostructure can generalize stable colloidal system for biomedical application such as hyperthermia.

Bio-application of synthesized magnetic aromatic organo-silane star polymer

In vitro cytotoxicity assay

MTT assay was used to assess the toxicity and biocompatibility of the synthesized magnetic aromatic organo-silane star polymer. This test was performed according to the method of Eivazzadeh-Keihan et al. [56–58]. First, human skin fibroblast cells (Hu02) were prepared from the cell bank of Pasteur Institute of Iran and cultured at 1×10^5 cell $well^{-1}$ in 96-well plate on the scaffolds under optimal conditions (37 °C, 5% CO_2 in humidified incubator). Next, the growth media (10% FBS) were removed and the cells were washed two times with PBS. New maintenance Roswell park memorial institute medium (RPMI) medium (10% FBS) containing 0.5, 5, 50, 500, and 1000 µg mL^{-1} of magnetic aromatic organo-silane star polymer was added and the cells were incubated for 24, 48, and 72 h. Quintet wells were analyzed for each concentration and column elution buffer was used as the control. A 10-µL solution of freshly prepared 5 mg mL^{-1} 3-(4,5-dimethyl-2-thiazolyl)-2,5-diphenyl-2H-tetrazolium

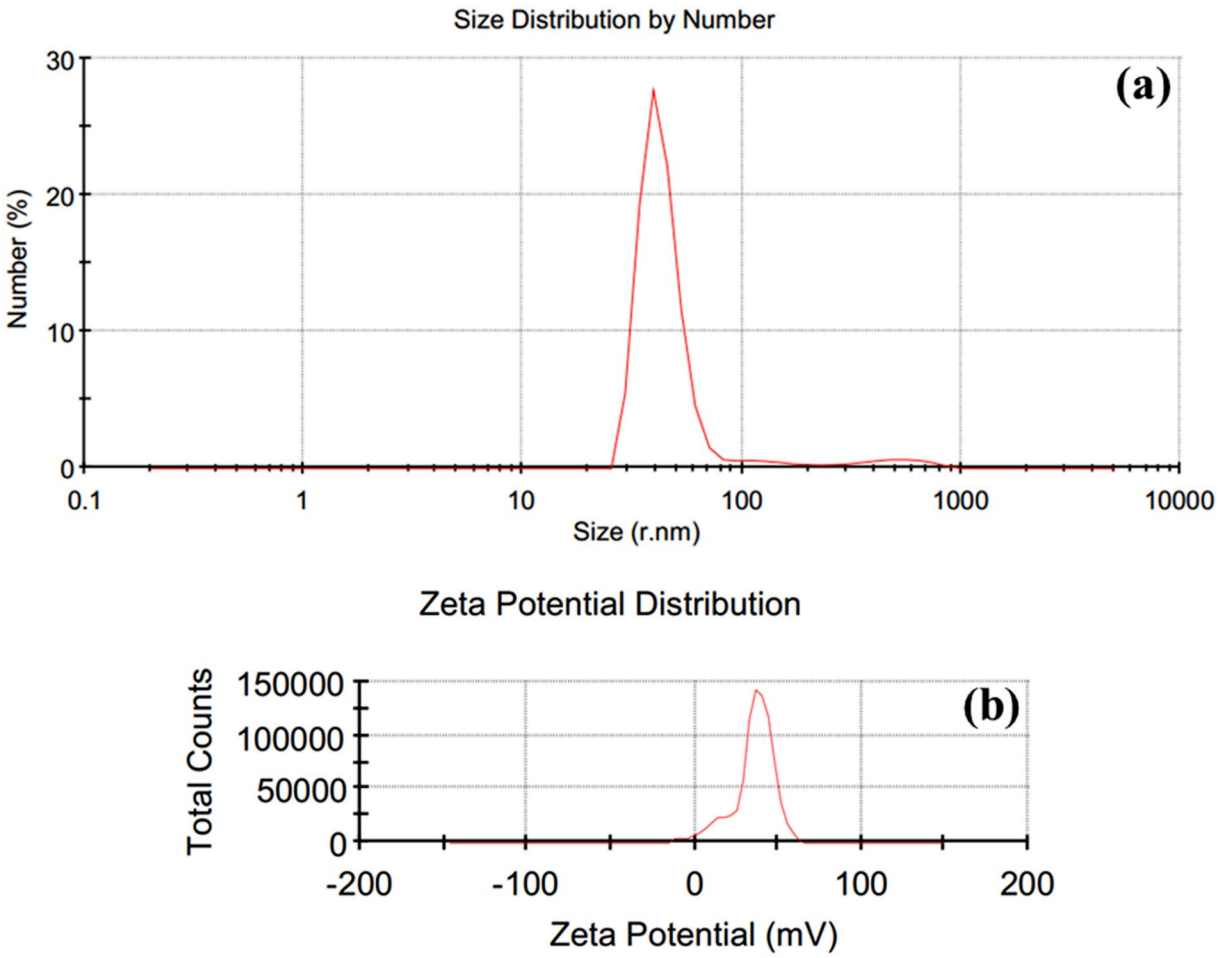

Fig. 8 **a** DLS histogram and **b** zetapotential histogram of magnetic aromatic organo-silane star polymer based on *p*-phenylenediamine

bromide (MTT) in phosphate-buffered saline (PBS) was added to each well and allowed to incubate for an additional 4 h. The media were removed and isopropanol was added at 100 µL well^{-1}. Plates were shaken gently to facilitate formazan crystal solubilization. The absorbance was measured at 545 nm using a microplate reader (STAT FAX 2100, BioTek, Winooski, USA) and the percentage of toxicity and cell viability were calculated using the following equations:

$$\text{Toxicity } (\%) = \left(1 - \frac{\text{mean OD of sample}}{\text{mean OD of control}}\right) \times 100, \quad (1)$$

$$\text{Cell viability } (\%) = 100\,(\%) - \text{Toxicity } (\%). \quad (2)$$

The IC_{50} of magnetic aromatic organo-silane star polymer was calculated according to the toxicity and concentration of the agents (Fig. 9a–d). The result was showed that the toxicity of this magnetic nanostructure at the highest concentration (1000 µg mL^{-1}) was 10.3%. Therefore, the percentage of cell viability in this concentration is 89.7% (Fig. 9a). However, IC_{50} values of synthesized polymer were > 1000 µg mL^{-1}. This rate of cell viability at this concentration indicates that this polymer is completely non-toxic and biocompatible with human skin fibroblast cells and can be used for biological applications such as skin tissue engineering and the construction of wound healing scaffolds. It is necessary to mention that the results are the average of three independent experiments. Also, the effect of magnetic aromatic organo-silane star polymer at concentration of 1000 µg mL^{-1} on cells morphology and shape was imaged with reverse microscope (Fig. 9c, d). Comparison of images of untreated cells with polymer-treated cells shows that the structure and morphology of these cells in the presence of the polymer has not changed significantly, which is another case that illustrates the biocompatibility of this material with Hu02 cells.

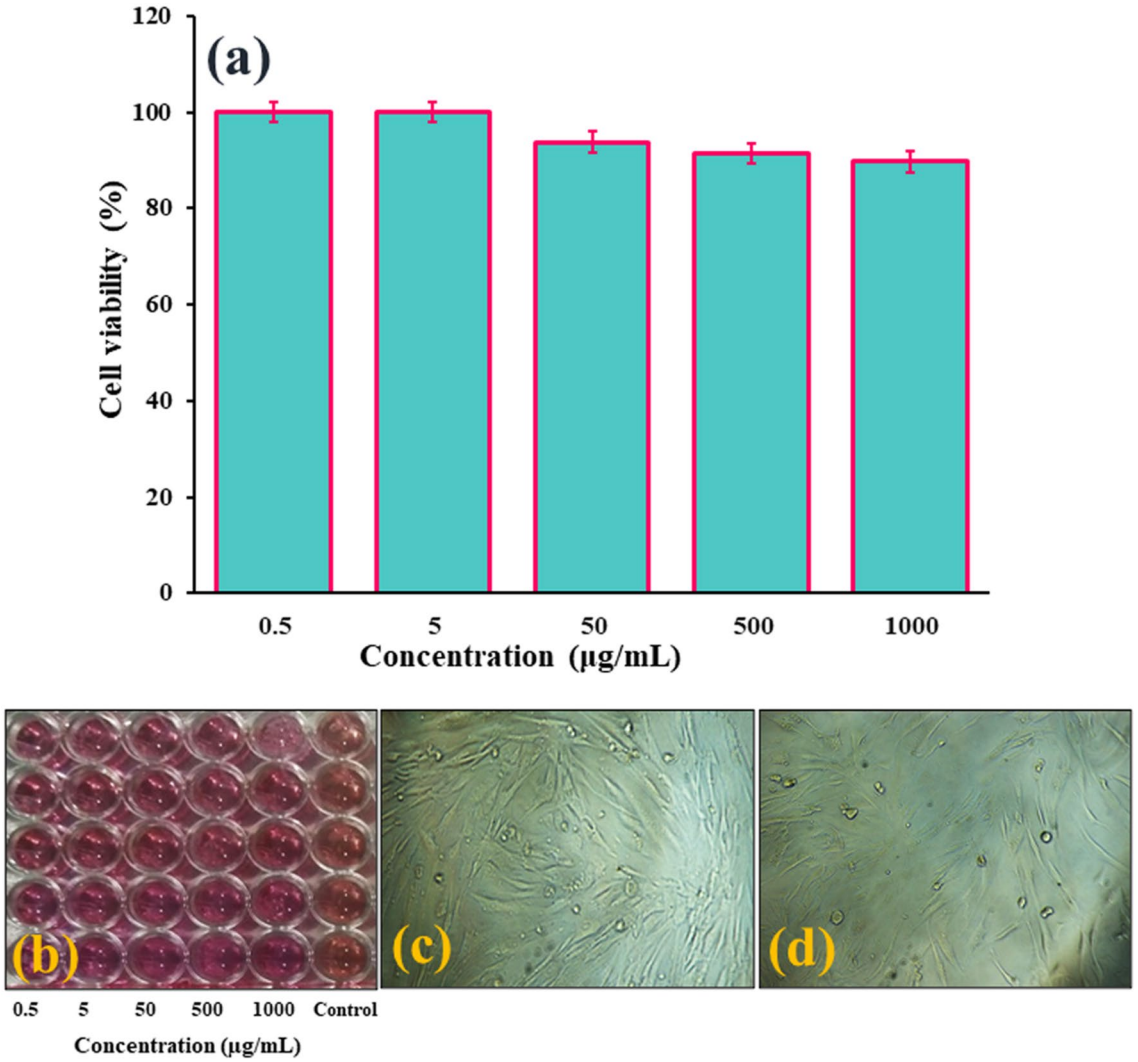

Fig. 9 **a** Cell viability histogram of untreated Hu02 cells for different concentration of magnetic aromatic organo-silane star polymer based on based on *p*-phenylenediamine, **b** image of microplate well from MTT assay on Hu02 cell line, **c** inverted microscope image of untreated Hu02 cell line morphology, and **d** inverted microscope image of untreated Hu02 cell line after treatment with magnetic aromatic organo-silane star polymer at concentration of 1000 µg mL^{-1}

Evaluating the heating capacities of magnetic aromatic organo-silane star polymer under the AMF

One of the interesting features of Fe_3O_4 MNPs is the ability to be manipulate by a magnetic field. This feature enables them to be a good candidate for several applications, including hyperthermia. In the presence of AMF, Fe_3O_4 MNPs generate heat. This heat generation is due to the Neel and Brownian relaxation, and hysteresis losses. The ability to turn Fe_3O_4 MNPs into a heating source in combination with their other features, such as their small size, ability for targeted delivery and potential for carrying drugs makes these nanoparticles for wide variety of application. Following these mentioned features and various applications to apply these magnetic nanoparticles and use their thermal power in therapeutic hyperthermia procedure, the consequential temperature increment needs to be controlled. Thermal power of a specific magnetic nanoparticles depends on their morphology and magnetic properties and the properties of the applied magnetic field. Herein, to evaluate the heating power of the magnetic aromatic organo-silane star polymer, during the 5- to 20-min intervals, different concentrations of designed magnetic nanocomposite (0.5 mg mL^{-1}, 1 mg mL^{-1}, 2 mg mL^{-1}, 5 mg mL^{-1}, 10 mg mL^{-1}) were exposed to AMF with different frequencies (100 MHz, 200 MHz, 300 MHz, 400 MHz). This process was accomplished during the 5- to 20-min intervals and for each sample the related temperature increment was recorded by forward looking infrared thermal camera. Following

the mentioned process to calculate the heating power of each sample, their specific absorption rate (SAR) was calculated using the following equation:

$$\mathrm{SAR} = \frac{C}{m}\frac{\Delta T}{\Delta t}, \tag{3}$$

where C is the specific heating capacity of the sample, m is the concentration of MNPs, T is the samples' temperature and t is time. Each sample was kept at 25 °C before the start of the hyperthermia process. As could be seen, the calculated values of SAR for each sample are determined in Fig. 10. While it may seem that the higher SAR is always preferable, due to efficiency of magnetic nanoparticles in hyperthermia, a specific amount of temperature increment and as well a determined amount of heating power is required. For example, in therapeutic hyperthermia process, tumor temperature should rise from 42 to 45 °C, because, in lower temperatures, tumor tissues will not sufficiently be damaged and higher temperatures can cause necrosis instead of apoptosis and as well, considerable to the surrounding healthy tissue [59]. In this study, maximum reported SAR was 66.18 W g^{-1} which happened at 0.5 mg mL^{-1} with an AMF frequency of 200 MHz. While these results did not indicate a clear pattern between AMF frequency and the heating power, it was determined that the concentration increment reduces the SAR value which as mentioned in previous studies, this is due to the dipole–dipole interaction of nanoparticles [60]. When concentration doubled from 0.5 to 1 mg mL^{-1}, maximum SAR reduces by 18.95% (Fig. 10). Moreover, maximum SAR reduction from 1 to 2 mg mL^{-1}, 2 to 5 mg mL^{-1} and 5 to 10 mg mL^{-1} was, respectively, 58.44%, 77.72% and 43.06%.

Evaluating the relevance between the maximum SAR value and sample concentration

As could be illustrated in Fig. 11, the relevance between the sample concentration and SAR value is not linear. This variation of heating power with both concentration and AMF frequency can be used to prepare a setup to reach the desired temperature for a wide range of applications. According to the obtained results, the calculated SAR value (66.18 W g^{-1}) under the right conditions can be enough to raise the temperature adequately to damage the tissue. In addition, it should be noted that in animal, clinical or in vivo assays, the final concentration inside target tissue determines the SAR value of the nanoparticles.

Conclusions

As a brief overview, in this study, statistical magnetic aromatic organo-silane star polymers were designed and synthesized based on surface functionalization of Fe_3O_4 MNPs using TEOS and CPTMS molecules and conducting the polymerization reaction between phenylenediamine derivatives and dichlorophenylsilane on their functionalized surfaces. To characterize the structural features, FT-IR, EDX, FE-SEM, TEM, XRD, TG, VSM analyses, and DLS and Zeta potential measurements were employed. The cytotoxicity and biocompatibility of magnetic aromatic organo-silane star polymer based on *p*-phenylenediamine as a model derivative with nanoplate morphology and considering structural features were evaluated using MTT assay. Different concentration of this new magnetic star polymer (0.5 µg mL^{-1}, 5 µg mL^{-1}, 50 µg mL^{-1}, 500 µg mL^{-1}, 1000 µg mL^{-1}) was prepared in this assay. Considering the highest concentration (1000 µg mL^{-1}),

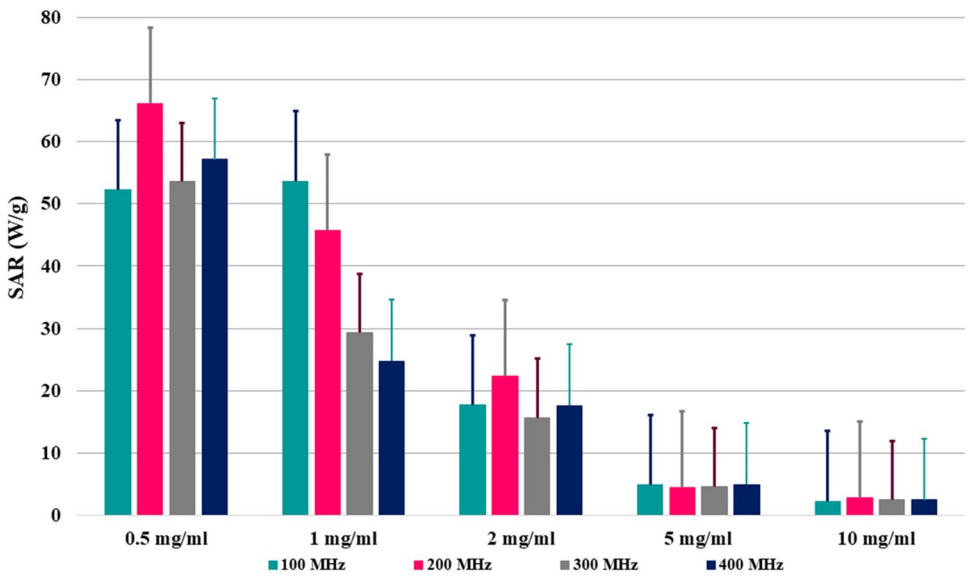

Fig. 10 Variation of calculated SAR values due to considering the different concentrations of designed magnetic nanocomposite and different frequencies

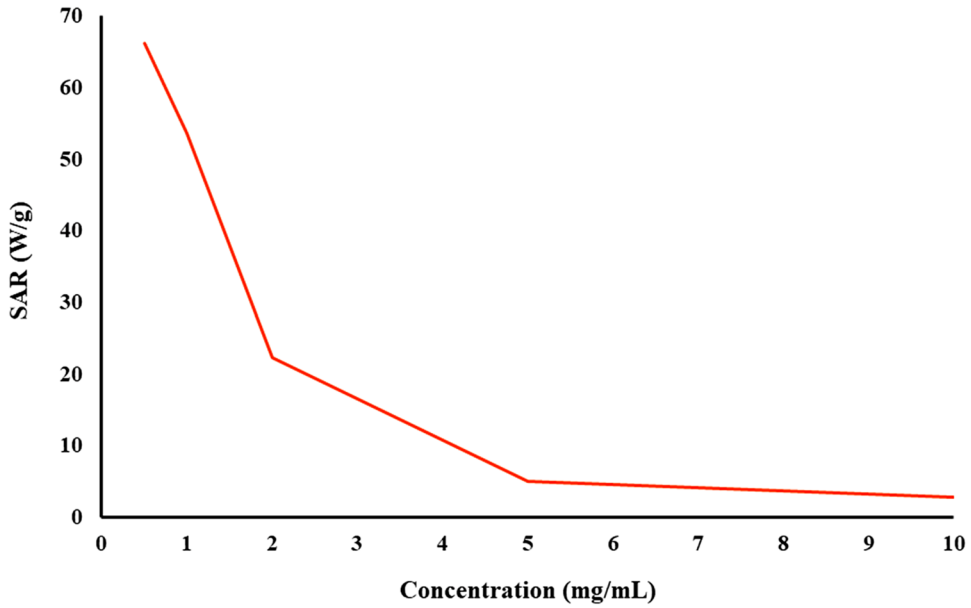

Fig. 11 Relevance curve between the SAR value and the sample concentration

the cell viability percentage was reported 89.7% and it was indicated that this new magnetic nanostructure had no toxic effect. Apart from cytotoxicity assay, the hyperthermia performance of model derivative was investigated under the alternating magnetic field (AMF), in different concentrations (0.5–10 mg mL^{-1}) and different frequencies (100–400 MHz). The maximum SAR value (66.18 W g^{-1}) was obtained from the lowest concentration (0.5 mg mL^{-1}) of magnetic star polymer sample and the relevance between the sample concentration and SAR value was not linear. Overall, it can be concluded that this magnetic star polymer could be considered for further in vivo investigations due to its biocompatibility and the calculated SAR value (66.18 W g^{-1}), because, it seems that, this magnetic star polymer can raise the temperature adequately to damage the targeted tissue under the right condition.

Supplementary Information The online version contains supplementary material available at https://doi.org/10.1007/s40097-021-00401-0.

Acknowledgements The authors gratefully acknowledge the partial support from the Research Council of the Iran University of Science and Technology (IUST) and Young Scientists Festival (YSF).

Declarations

Conflict of interest The authors whose names are listed in this article have no competing interests or other conflict of interests that might be perceived to influence the results and/or discussion reported in this paper.

References

1. Ren, J.M., et al.: Star polymers. Chem. Rev. **116**, 6743–6836 (2016)
2. Eivazzadeh-Keihan, R., Radinekiyan, F., Maleki, A., Bani, M.S., Azizi, M.: A new generation of star polymer: magnetic aromatic polyamides with unique microscopic flower morphology and in vitro hyperthermia of cancer therapy. J. Mater. Sci. **55**, 319–336 (2020)
3. Aloorkar, N., Kulkarni, A., Patil, R., Ingale, D.: Star polymers: an overview. Int. J. Pharm. Sci. Nanotechnol. **5**, 1675–1684 (2012)
4. Wu, W., He, Q., Jiang, C.: Magnetic iron oxide nanoparticles: synthesis and surface functionalization strategies. Nanoscale Res. Lett. **3**, 397 (2008)
5. Ali, A., et al.: Synthesis, characterization, applications, and challenges of iron oxide nanoparticles. Nanotechnol. Sci. Appl. **9**, 49 (2016)
6. Eivazzadeh-Keihan, R., et al.: Synthesis of core-shell magnetic supramolecular nanocatalysts based on amino-functionalized calix [4] arenes for the synthesis of 4H-chromenes by ultrasonic waves. ChemistryOpen **9**, 735–742 (2020)
7. Asgharnasl, S., Eivazzadeh-Keihan, R., Radinekiyan, F., Maleki, A.: Preparation of a novel magnetic bionanocomposite based on factionalized chitosan by creatine and its application in the synthesis of polyhydroquinoline, 1, 4-dyhdropyridine and 1, 8-dioxodecahydroacridine derivatives. Int. J. Biol. Macromol. **144**, 29–46 (2020)
8. Hajizadeh, Z., Maleki, A., Rahimi, J., Eivazzadeh-Keihan, R.J.S.: Halloysite nanotubes modified by Fe_3O_4 nanoparticles and applied as a natural and efficient nanocatalyst for the symmetricalhantzsch reaction. SILICON **12**, 1247–1256 (2020)
9. Esmaeili, M.S., Varzi, Z., Eivazzadeh-Keihan, R., Maleki, A., Ghafuri, H.: Design and development of natural and biocompatible raffinose-Cu_2O magnetic nanoparticles as a heterogeneous nanocatalyst for the selective oxidation of alcohols. Mol. Catal. **492**, 111037 (2020)
10. Huang, C.-C., et al.: New insight on optical and magnetic Fe_3O_4 nanoclusters promising for near infrared theranostic applications. Nanoscale **7**, 12689–12697 (2015)
11. Eivazzadeh-Keihan, R., Radinekiyan, F., Asgharnasl, S., Maleki, A., Bahreinizad, H.: A natural and eco-friendly magnetic nanobiocomposite based on activated chitosan for heavy metals adsorption and the in-vitro hyperthermia of cancer therapy. J. Mater. Res. Technol. **9**, 12244–12259 (2020)

12. Mokhtarzadeh, A., et al.: Nanomaterial-based biosensors for detection of pathogenic virus. Trends. Anal. Chem. **97**, 445–457 (2017)
13. Eivazzadeh-Keihan, R., et al.: Dengue virus: a review on advances in detection and trends–from conventional methods to novel biosensors. Microchim. Acta **186**, 329 (2019)
14. Eivazzadeh-Keihan, R., et al.: Recent progress in optical and electrochemical biosensors for sensing of *Clostridium botulinum* neurotoxin. Trends. Anal. Chem. **103**, 184–197 (2018)
15. Mohammadinejad, A., et al.: Development of biosensors for detection of alpha-fetoprotein: as a major biomarker for Hepatocellular carcinoma. Trends. Anal. Chem. **130**, 115961 (2020)
16. Eivazzadeh-Keihan, R., Pashazadeh, P., Hejazi, M., de la Guardia, M., Mokhtarzadeh, A.: Recent advances in nanomaterial-mediated bio and immune sensors for detection of aflatoxin in food products. Trends. Anal. Chem. **87**, 112–128 (2017)
17. Eivazzadeh-Keihan, R., et al.: Recent advances on nanomaterial based electrochemical and optical aptasensors for detection of cancer biomarkers. Trends. Anal. Chem. **100**, 103–115 (2018)
18. Eivazzadeh-Keihan, R., et al.: Carbon based nanomaterials for tissue engineering of bone: building new bone on small black scaffolds: a review. J. Adv. Res. **18**, 185–201 (2019)
19. Rao, W., Deng, Z.-S.: A review of hyperthermia combined with radiotherapy/chemotherapy on malignant tumors. Crit. Rev. Biomed. Eng. **38**, 101–106 (2010)
20. Guibert, C., Dupuis, V., Peyre, V., Fresnais, J.: Hyperthermia of magnetic nanoparticles: experimental study of the role of aggregation. J. Phys. Chem. C **119**, 28148–28154 (2015)
21. Ahmad, A., et al.: Hyperbranched polymer-functionalized magnetic nanoparticle-mediated hyperthermia and niclosamide bimodal therapy of colorectal cancer cells. ACS Biomater. Sci. Eng. **6**, 1102–1111 (2019)
22. Li, T.-J., et al.: In vivo anti-cancer efficacy of magnetite nanocrystal-based system using locoregional hyperthermia combined with 5-fluorouracil chemotherapy. Biomaterials **34**, 7873–7883 (2013)
23. Zamora-Mora, V., et al.: Magnetic core–shell chitosan nanoparticles: rheological characterization and hyperthermia application. Carbohydr. Polym. **102**, 691–698 (2014)
24. Fadhilah, H., Saepudin, E., Khalil, M. In: AIP conference proceedings 2020, vol. 1, p. 040003. AIP Publishing LLC
25. Shen, L., Li, B., Qiao, Y.: Fe_3O_4 nanoparticles in targeted drug/gene delivery systems. Materials **11**, 324 (2018)
26. Boyer, C., Whittaker, M.R., Bulmus, V., Liu, J., Davis, T.P.: The design and utility of polymer-stabilized iron-oxide nanoparticles for nanomedicine applications. NPG Asia Mater. **2**, 23–30 (2010)
27. Arias, J.L., Reddy, L.H., Couvreur, P.: Fe_3O_4/chitosan nanocomposite for magnetic drug targeting to cancer. J. Mater. Chem. **22**, 7622–7632 (2012)
28. Eivazzadeh-Keihan, R., et al.: A novel biocompatible core-shell magnetic nanocomposite based on cross-linked chitosan hydrogels for in vitro hyperthermia of cancer therapy. Int. J. Biol. Macromol. **140**, 407–414 (2019)
29. Furlan, D.M., et al.: Sisal cellulose and magnetite nanoparticles: formation and properties of magnetic hybrid films. J. Mater. Res. Technol. **8**, 2170–2179 (2019)
30. Diaz-Bleis, D., Vales-Pinzón, C., Freile-Pelegrín, Y., Alvarado-Gil, J.: Thermal characterization of magnetically aligned carbonyl iron/agar composites. Carbohydr. Polym. **99**, 84–90 (2014)
31. Seenuvasan, M., et al.: Fabrication, characterization and application of pectin degrading Fe_3O_4–SiO_2 nanobiocatalyst. Mater. Sci. Eng. C **33**, 2273–2279 (2013)
32. Le, T.T.H., et al.: Optimizing the alginate coating layer of doxorubicin-loaded iron oxide nanoparticles for cancer hyperthermia and chemotherapy. J. Mater. Sci. **53**, 13826–13842 (2018)
33. Li, T.-J., et al.: Handheld energy-efficient magneto-optical real-time quantitative PCR device for target DNA enrichment and quantification. NPG Asia Mater. **8**, e277 (2016)
34. Adebayo, L.L., et al.: Facile preparation and enhanced electromagnetic wave absorption properties of Fe_3O_4@ PVDF nanocomposite. J. Mater. Res. Technol. **9**, 2513–2521 (2020)
35. Li, J., et al.: Three-dimensional graphene supported Fe_3O_4 coated by polypyrrole toward enhanced stability and microwave absorbing properties. J. Mater. Res. Technol. **9**, 762–772 (2020)
36. Bani, M.S., et al.: Casein-coated iron oxide nanoparticles for in vitro hyperthermia for cancer therapy. Spin **9**, 1940003 (2019)
37. Marutani, E., et al.: Surface-initiated atom transfer radical polymerization of methyl methacrylate on magnetite nanoparticles. Polymer **45**, 2231–2235 (2004)
38. Hu, H., et al.: Preparation of amino-functionalized magnetite nanoclusters by ring-opening polymerization and application for targeted magnetic resonance imaging. J. Mater. Sci. **48**, 7686–7695 (2013)
39. Rana, S., Jadhav, N.V., Barick, K., Pandey, B., Hassan, P.: Polyaniline shell cross-linked Fe_3O_4 magnetic nanoparticles for heat activated killing of cancer cells. Dalton. Trans. **43**, 12263–12271 (2014)
40. Ahmad, A., Khan, F., Mishra, R.K., Khan, R.: Precision cancer nanotherapy: evolving role of multifunctional nanoparticles for cancer active targeting. J. Med. Chem. **6**, 10475–10496 (2019)
41. Gupta, A., et al.: Correction to "Nanocarrier composed of magnetite core coated with three polymeric shells mediates LCS-1 delivery for synthetic lethal therapy of BLM-defective colorectal cancer cells." Biomacromol **20**, 4623–4623 (2019)
42. Eivazzadeh-Keihan, R., Bahrami, N., Radinekiyan, F., Maleki, A., Mahdavi, M.: Palladium-coated thiourea core-shell nanocomposite as a new, efficient, and magnetic responsive nanocatalyst for the Suzuki-Miyaura coupling reactions. Mater. Res. Express **8**, 026102 (2021)
43. Stöber, W., Fink, A., Bohn, E.: Controlled growth of monodisperse silica spheres in the micron size range. J. Colloid Interface Sci. **26**, 62–69 (1968)
44. Ji, L., et al.: Facile synthesis of multiwall carbon nanotubes/iron oxides for removal of tetrabromobisphenol A and Pb (II). J. Mater. Chem. **22**, 15853–15862 (2012)
45. Villa, S., Riani, P., Locardi, F., Canepa, F.: Functionalization of Fe_3O_4 NPs by silanization: use of amine (APTES) and thiol (MPTMS) silanes and their physical characterization. Materials **9**, 826 (2016)
46. Safaiee, M., Zolfigol, M.A., Afsharnadery, F., Baghery, S.: Synthesis of a novel dendrimer core of oxo-vanadium phthalocyanine magnetic nano particles: as an efficient catalyst for the synthesis of 3, 4-dihydropyrano [c] chromenes derivatives under green condition. RSC Adv. **5**, 102340–102349 (2015)
47. Farahi, M., Karami, B., Keshavarz, R., Khosravian, F.: Nano-Fe_3O_4@ SiO_2-supported boron sulfonic acid as a novel magnetically heterogeneous catalyst for the synthesis of pyrano coumarins. RSC Adv. **7**, 46644-46650 (2017)
48. Vieira, E.G., et al.: Synthesis and characterization of 3-[(thiourea)-propyl]-functionalized silica gel and its application in adsorption and catalysis. N. J. Chem. **37**, 1933–1943 (2013)
49. Lu, X.-W., Wu, W., Chen, J.-F., Zhang, P.-Y., Zhao, Y.-B.: Preparation of polyaniline nanofibers by high gravity chemical oxidative polymerization. Ind. Eng. Chem. Res. **50**, 5589–5595 (2011)
50. Halim, M., Hudaya, C., Kim, A.-Y., Lee, J.K.: Phenyl-rich silicone oil as a precursor for SiOC anode materials for long-cycle and high-rate lithium ion batteries. J. Mater. Chem. A **4**, 2651–2656 (2016)
51. Launer, P.: Infrared analysis of organosilicon compounds: spectra-structure correlations. Inc. Burnt Hills, New York (1987)

52. Zhou, H., Zhou, Q., Zhou, Q., Ni, L., Chen, Q.: Highly heat resistant and thermo-oxidatively stable borosilane alkynyl hybrid polymers. RSC Adv. **5**, 12161–12167 (2015)
53. Mouradzadegun, A., Ganjali, M.R., Mostafavi, M.A.: Design and synthesis of a magnetic hierarchical porous organic polymer: a new platform in heterogeneous phase-transfer catalysis. Appl. Organomet. Chem. **32**, e4214 (2018)
54. Wei, S., et al.: Multifunctional composite core–shell nanoparticles. Nanoscale **3**, 4474–4502 (2011)
55. Darwish, M.S., Nguyen, N.H., Ševců, A., Stibor, I.: Functionalized magnetic nanoparticles and their effect on *Escherichia coli* and *Staphylococcus aureus*. J. Nanomater. **2015,** 416012-416022 (2015)
56. Eivazzadeh-Keihan, R., Radinekiyan, F., Madanchi, H., Aliabadi, H.A.M., Maleki, A.: Graphene oxide/alginate/silk fibroin composite as a novel bionanostructure with improved blood compatibility, less toxicity and enhanced mechanical properties. Carbohydr. Polym. **248**, 116802 (2020)
57. Eivazzadeh-Keihan, R., et al.: Chitosan hydrogel/silk fibroin/Mg $(OH)_2$ nanobiocomposite as a novel scaffold with antimicrobial activity and improved mechanical properties. Sci. Rep. **11**, 1–13 (2021)
58. Eivazzadeh-Keihan, R., et al.: Alginate hydrogel-polyvinyl alcohol/silk fibroin/magnesium hydroxide nanorods: a novel scaffold with biological and antibacterial activity and improved mechanical properties. Int. J. Biol. Macromol. **162**, 1959–1971 (2020)
59. Kaushik, K., Kaushal, N., Kalla, N.R.: Conversion of apoptosis to necrosis and the corresponding alteration in the oxidative milieu of male germ cells of rat under acute heat stress: an experimental study. Int. J. Reprod. Biomed. **16**, 577 (2018)
60. Hatamie, S., et al.: Graphene/cobalt nanocarrier for hyperthermia therapy and MRI diagnosis. Colloids Surf. B **146**, 271–279 (2016)